Supplementary Information

Importance of choosing the right polymerization method for in situ preparation of semiconducting nanoparticles from P3HT block copolymer

In-Hwan Lee and Tae-Lim Choi*

Department of Chemistry, Seoul National University, Seoul, 08826, Korea

E-mail: tlc@snu.ac.kr

Table of contents

General experimental considerations

NMR spectra were recorded by Varian/Oxford As-500 (500 MHz for ^{1}H, 125 MHz for ^{13}C) and Agilent 400-MR DD2 Magnetic Resonance System (400 MHz for ^{1}H, 100 MHz for ^{13}C). THF Gel permeation chromatography (GPC) for polymer molecular weight analysis was carried out with Waters system (1515 pump, 2414 refractive index detector, and 2489 UV detector) and Shodex GPC LF-804 column eluted with THF (GPC grade, Honeywell Burdick & Jackson). Flow rate was 1.0 mL/min, and temperature of the column was maintained at 35 ℃. Samples were diluted in 0.001-0.005 wt% by THF and filtered with a 0.20 μm PTFE filter before injection into the GPC. UV/Vis spectra were obtained by Jasco Inc. UV-vis Spectrometer V-650. Typical concentration of UV/vis measurement was 0.002 mg/ml in $CHCl_3$. Powder X-ray diffraction (XRD) was performed by the National Instrumentation Center for Environmental Management (NICEM) at SNU using D8 Discover with GADDS (Bruker, Germany). Dynamic light scattering (DLS) data were obtained by Malvern Zetasizer Nano ZS. Differential scanning calorimetry (DSC) was carried out under N_2 gas at a scan rate of 10 ℃/min with Q50 and Q10 model devices, respectively, from TA Instruments. Cyclic voltammetry (CV) measurements were carried out on a CHI 660 Electrochemical Analyzer (CH Instruments, Insc., Texas, USA). Sonication was carried out with Powersonic 410 model devices from Hwashin Tech operating at AC220V 50/60 Hz and 500 W. Matrix-assisted laser desorption ionization time-of-flight (MALDI-TOF) mass spectra were collected on a Bruker Daltonics Autoflex II spectrometer using dithranol as a matrix. Monomer conversion was identified using a Hewlett Packard 5890 Gas Chromatograph-Mass spectrometry (GC-MS).

(1) Atomic Force Microscopy (AFM)

The atomic force microscopy experiments were performed with a thin film prepared by spin-coating one drop of the polymer solution (0.05-0.1 mg polymer/mL chloroform, spinning rate = 3000 rpm for 30 sec) on freshly prepared highly ordered pyrolytic graphite (HOPG) substrates. Multimode 8 and Nanoscope V controller (Veeco Instrument) were used for AFM imaging. AFM images were obtained on tapping mode using non-contact mode tips from Nanoworld (Pointprobe® tip, NCHR type) with the spring constant of 42 Nm^{-1} and tip radius of $\leq$ 8 nm.

(2) Transmission Electron Microscopy (TEM)

The samples for TEM were prepared by drop-casting 10 μL aliquots of the polymer solution (0.005 mg polymer/mL chloroform) onto a carbon coated copper grid which was placed on a piece of paper to get rid of excess solvent. This polymer thin film was dried in the clean desiccator. The images were obtained by JEM-2100 operating at 200 kV accelerating voltage with ORIUS-SC 600 CCD camera or ORIUS-SC 1000 CCD camera (Gatan, Inc.) in the National Center for Inter-University Research Facility (NCIRF) at SNU.

(3) Cyclic Voltammetry (CV)

Cyclic voltammetry (CV) measurement was carried out at the room temperature on a CHI 660 Electrochemical Analyzer (CH Instruments, Insc., Texas, USA) using a degassed acetonitrile solution of tetrabutylammonium hexafluorophosphate (Bu_4NPF_6, 0.1 M). The thin film was prepared by drop-casting 10 μL aliquot of the polymer solution onto the glassy carbon electrode. Cyclic voltammogram was recorded using the polymer-coated working electrode and a reference electrode of Ag/Ag^+ (0.1 M $AgNO_3$ in acetonitrile) with a platinum wire counter electrode at a scan rate of 50 mV/s. The absolute energy level was obtained using ferrocene/ferrocenium as an internal standard. The oxidation potential of ferrocene was regarded as -4.8 eV.

Materials

Without additional notes, all reagents were commercially available and used without further purification. THF was distilled over sodium and benzophenone. 2-Bromo-5-iodo-3-hexylthiophene,[S1] (*o*-tolyl)Ni(PPh_3)$_2$Br,[S2-3] (*o*-tolyl)Ni(dppe)Br[10d] were prepared according to literature methods. (*o*-Tolyl)Ni(dppp)Br was in situ prepared from (*o*-tolyl)Ni(PPh_3)$_2$Br according to literature method.[10c,f] PT homopolymer was prepared according to literature method.[5c]

(1) P3HT homopolymer

P3HT with M_n = 17.1 kg/mol, PDI = 1.12 (THF SEC, PS standard) was prepared in 57% yield by the conventional KCTP method[8] (purification: precipitated into MeOH followed by Soxhlet extraction with MeOH and *n*-hexane).

(2) General procedure for the synthesis of P3HT-*b*-PT and *o*-tolyl-P3HT-*b*-PT

Two round-bottomed two-neck flasks were flame-dried under reduced pressure and cooled to room temperature. The dried flasks were backfilled with argon. 2-bromo-5-iodo-3-hexylthiophene (1 equiv) was placed in one of the flasks under argon flow. After addition of dry THF (0.1 M) into the flask, 1.3 M *i*-PrMgCl-LiCl complex in THF (1 equiv) was added, and the mixture was stirred for 30 min at 0 °C (**solution 1**). Meanwhile, 2,5-dibromothiophene and naphthalene (internal standard) were placed in the other flask under argon flow. After addition of dry THF (0.1 M) into the flask, 1.3 M *i*-PrMgCl-LiCl complex in THF (1 equiv relative to 2,5-dibromothiophene) was added, and the mixture was stirred for 2 h at room temperature (**solution 2**). After completion of the preparation of Grignard reagent, Ni catalyst (2 mol% relative to 2-bromo-5-iodo-3-hexylthiophene) was added in **solution 1** under argon flow. Polymerization underwent for 30 minutes at room temperature, and an aliquot of **solution 1** was taken to check the M_n and PDI values of the first block, P3HT. At the same time, an aliquot of **solution 2** was taken to check the efficiency of Grignard exchange reaction of 2,5-dibromothiophene. Next, **solution 2** was transferred into **solution 1** via a cannula to synthesize the block copolymer, and it was stirred for 1 h at room temperature. After completion of the reaction, an aliquot was taken to check the conversion of Grignard reagent from 2,5-dibromothiophene. Finally, the polymerization was quenched by the addition of 6 *N* HCl (aq) to the resulting solution, and it was diluted with MeOH to give the black precipitates. The precipitates were collected by filtration and washed with H_2O and MeOH, and they were dried.

Figure S1. ^{1}H NMR spectra of P3HT, P3HT-*b*-PT, and *o*-tolyl-P3HT-*b*-PT

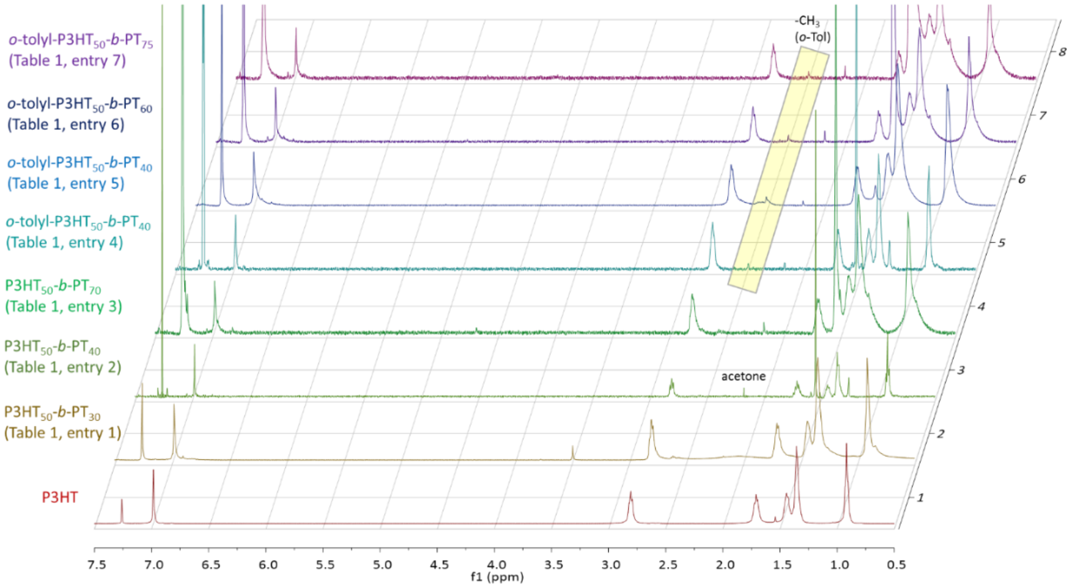

Figure S2. Representative SEC trace and MALDI-TOF spectrum of *o*-tolyl-P3HT (Table 1, entry 5)

(a) SEC (THF, PS standard)

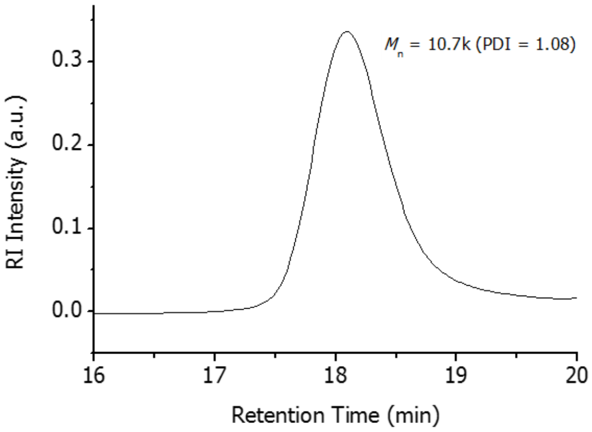

(b) MALDI-TOF

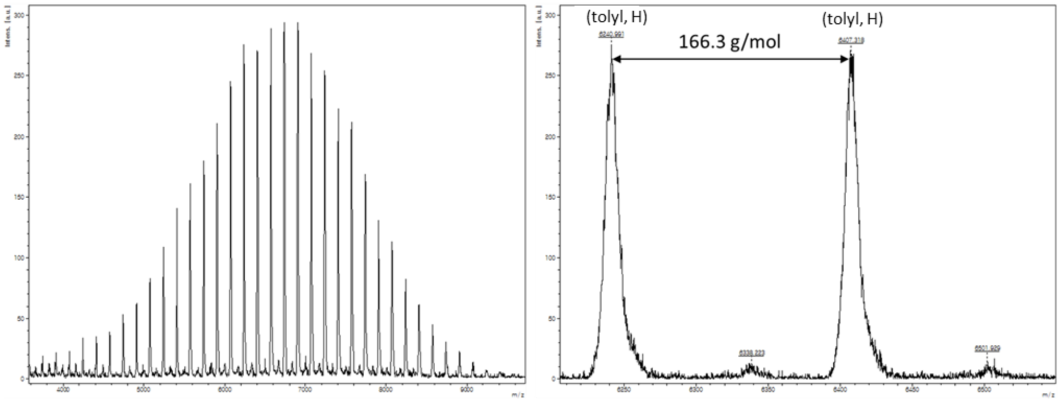

Figure S3. Estimation on DP of PT by GC conversion of M5 and M6

	M5/Ni ratio	conversion of **M5**[a]	conversion of **M6**[b]	DP of PT[c]
P3HT$_{50}$-*b*-PT$_{30}$ (Table 1, entry 1)	30/1	97.8%	75.8%	22
P3HT$_{50}$-*b*-PT$_{40}$ (Table 1, entry 2)	40/1	92.7%	84.6%	31
P3HT$_{50}$-*b*-PT$_{70}$ (Table 1, entry 3)	70/1	99.9%	89.7%	63
o-tolyl-P3HT$_{50}$-*b*-PT$_{40}$ (Table 1, entry 4)	40/1	91.6%	80.2%	29
o-tolyl-P3HT$_{50}$-*b*-PT$_{40}$ (Table 1, entry 5)	40/1	95.3%	77.8%	30
o-tolyl-P3HT$_{50}$-*b*-PT$_{60}$ (Table 1, entry 6)	60/1	95.3%	82.9%	47
o-tolyl-P3HT$_{50}$-*b*-PT$_{75}$ (Table 1, entry 7)	75/1	97.0%	81.2%	59

[a] Measured by gas chromatography–mass spectrometry (GC-MS). Calibration of analytes was carried out using naphthalene as a standard.
[b] Measured by gas chromatography–mass spectrometry (GC-MS) using naphthalene as the internal standard.
[c] Calculated using the formula (DP of PT = **M5**/Ni ratio * conversion of **M5** * conversion of **M6**).

Representative GC data for *o*-tolyl-P3HT$_{50}$-*b*-PT$_{40}$ (Table 1, entry 4)

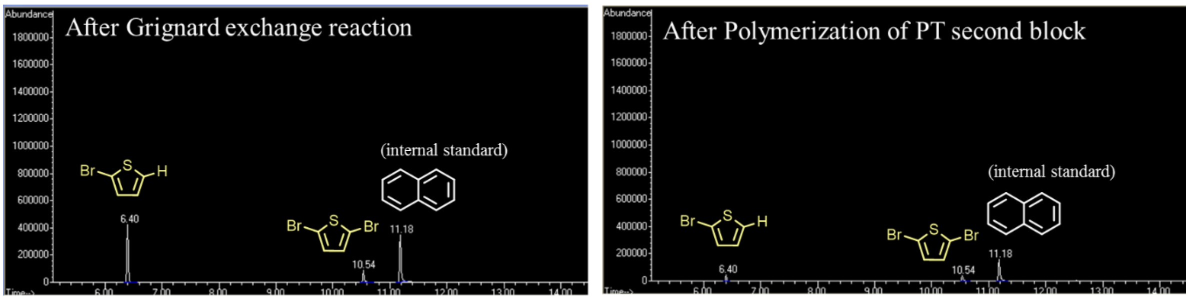

Figure S4. AFM (with height profile) and TEM images of P3HT-*b*-PT and *o*-tolyl-P3HT-*b*-PT

(a) P3HT$_{50}$-*b*-PT$_{30}$ (Table 1, entry 1)

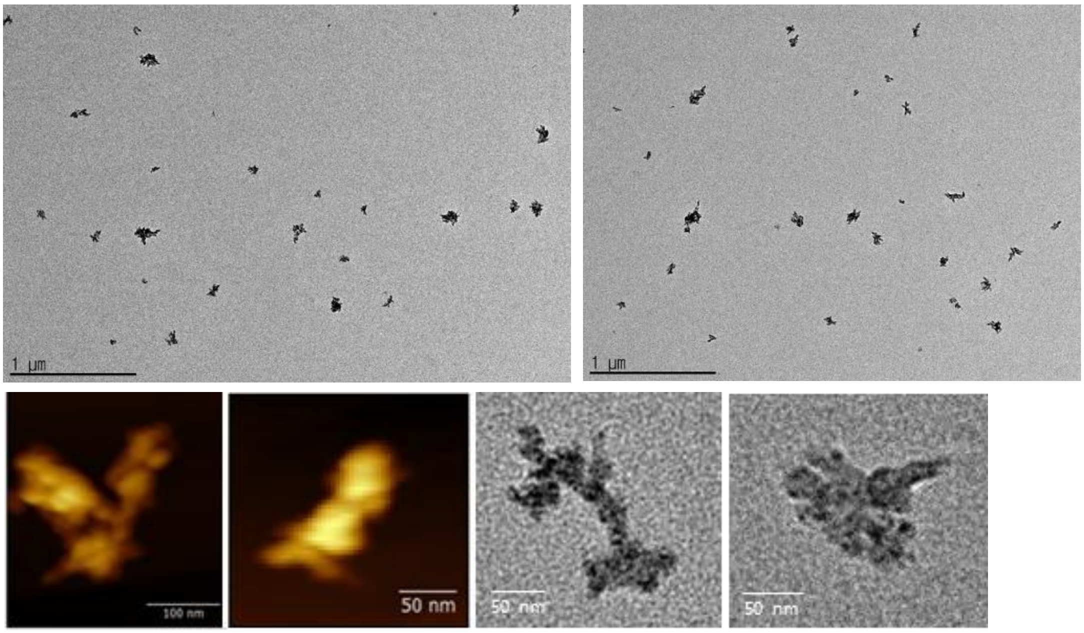

(b) P3HT$_{50}$-*b*-PT$_{40}$ (Table 1, entry 2)

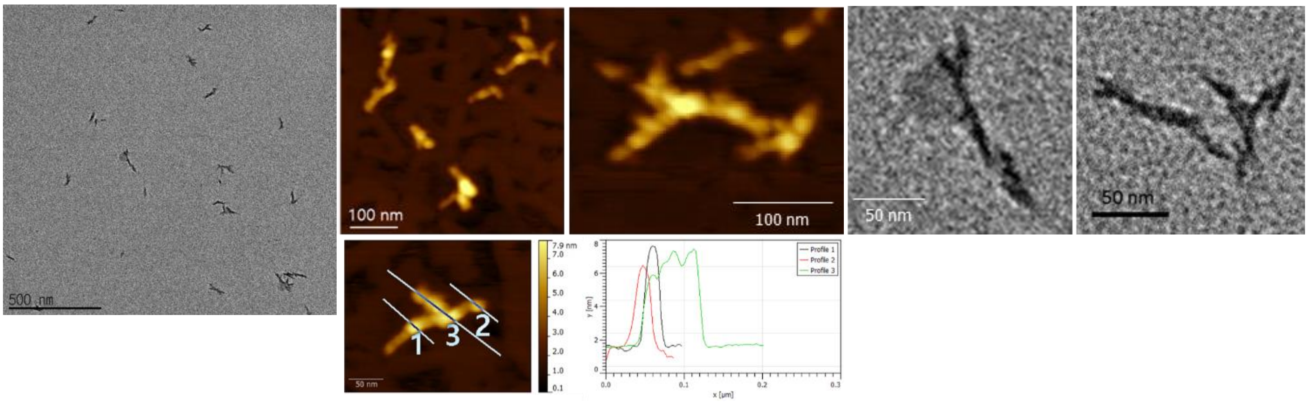

(c) P3HT$_{50}$-*b*-PT$_{70}$ (Table 1, entry 3)

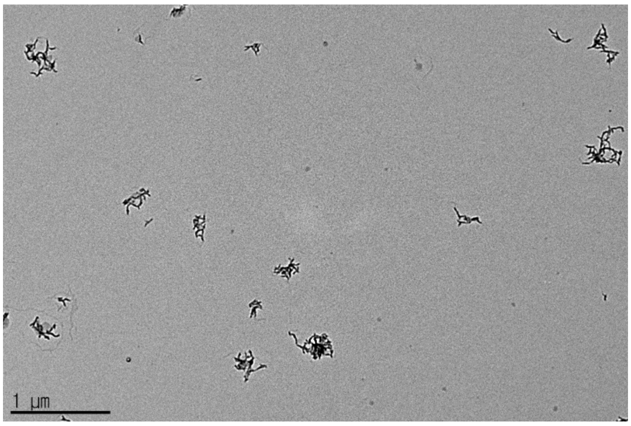

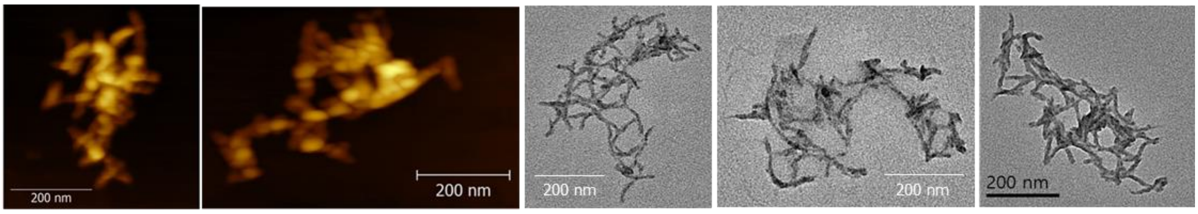

(d) *o*-tolyl-P3HT$_{50}$-*b*-PT$_{40}$ (Table 1, entry 4)

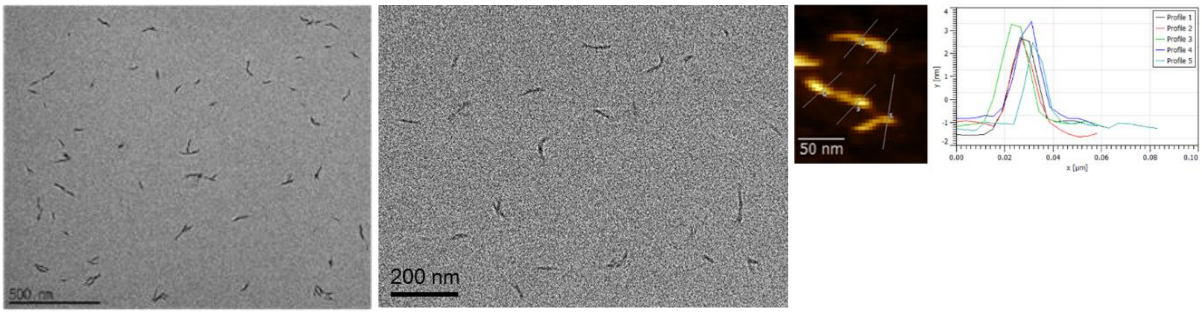

(e) *o*-tolyl-P3HT$_{50}$-*b*-PT$_{60}$ (Table 1, entry 6)

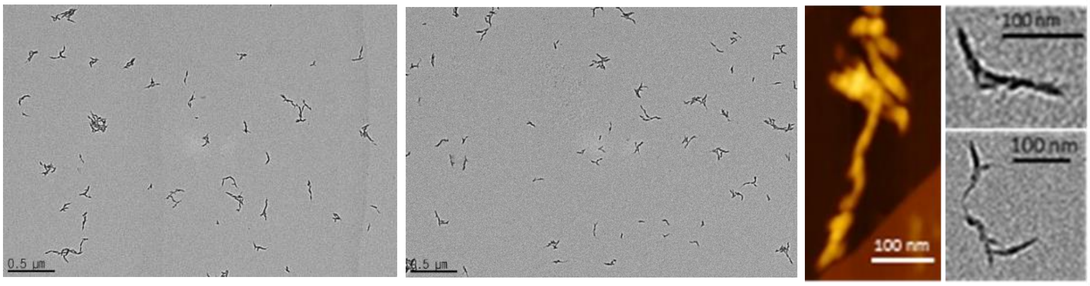

(f) *o*-tolyl-P3HT$_{50}$-*b*-PT$_{75}$ (Table 1, entry 7)

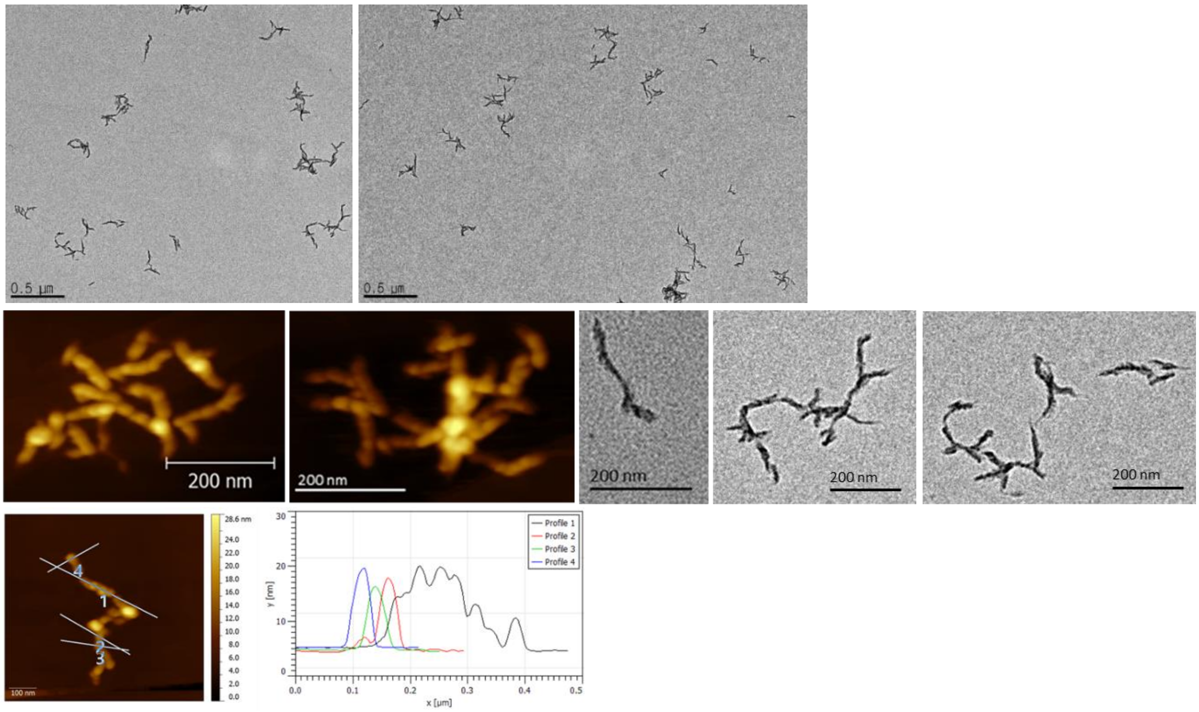

(g) Average height of nanoparticles from AFM images

	average height (nm)	standard deviation (nm)
P3HT$_{50}$-*b*-PT$_{30}$ (Table 1, entry 1)	25.3	6.4
P3HT$_{50}$-*b*-PT$_{40}$ (Table 1, entry 2)	4.7	1.4
P3HT$_{50}$-*b*-PT$_{70}$ (Table 1, entry 3)	14.0	5.3
o-tolyl-P3HT$_{50}$-*b*-PT$_{40}$ (Table 1, entry 4)	4.4	0.8
o-tolyl-P3HT$_{50}$-*b*-PT$_{40}$ (Table 1, entry 5)	4.2	1.1
o-tolyl-P3HT$_{50}$-*b*-PT$_{60}$ (Table 1, entry 6)	5.4	1.4
o-tolyl-P3HT$_{50}$-*b*-PT$_{75}$ (Table 1, entry 7)	12.4	3.1

P3HT$_{50}$-*b*-PT$_{30}$ (Table 1, entry 1)

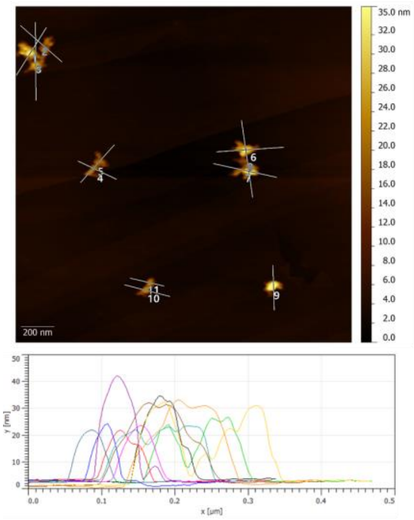

entry	height (nm)
1	19.4
2	21
3	39.4
4	30.1
5	28.9
6	31.2
7	29.7
8	20.5
9	18.9
10	20.9
11	23.4
12	21.5
13	18.4
14	31.5
avg	**25.3**
std	**6.4**

P3HT$_{50}$-*b*-PT$_{40}$ (Table 1, entry 2)

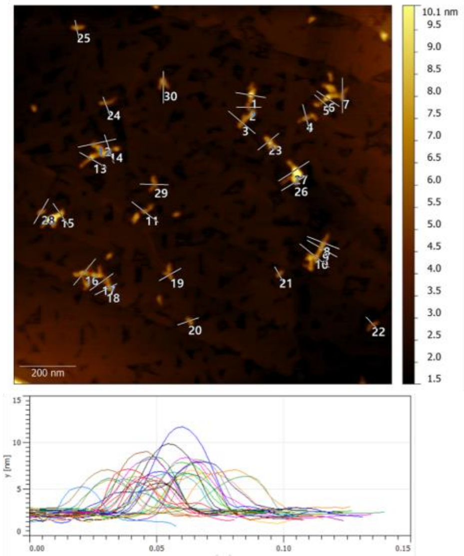

entry	height (nm)
1	7.4
2	3
3	4.1
4	4.1
5	3.1
6	6.2
7	3.7
8	5
9	5.9
10	5.9
11	4
12	4
13	5.6
14	3.6
15	5.6
16	4.8
17	3.2
18	4.1
19	3.8
20	4.4
21	3.7
22	3.7
23	5.7
24	3.6
25	5.1
26	5.6
27	9.2
28	4.1
29	3.6
30	4.9
avg	**4.7**
std	**1.4**

P3HT$_{50}$-*b*-PT$_{70}$ (Table 1, entry 3)

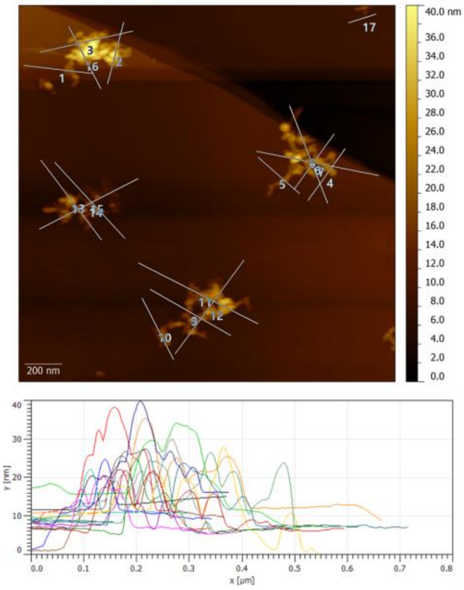

entry	height (nm)
1	8.6
2	27
3	18.3
4	13.6
5	11.1
6	13.9
7	9.8
8	6.4
9	12.79
10	23.19
11	13.29
12	9
13	8.2
14	16.4
15	14.3
16	6.1
17	9.7
18	13.3
19	19.2
20	15.7
21	7.3
22	15.2
23	17.2
24	15
25	22.7
26	15.4
27	15.3
28	10.2
29	9.3
30	18.5
31	9.8
32	23.7
avg	**14.0**
std	**5.3**

o-tolyl-P3HT$_{50}$-*b*-PT$_{40}$ (Table 1, entry 4)

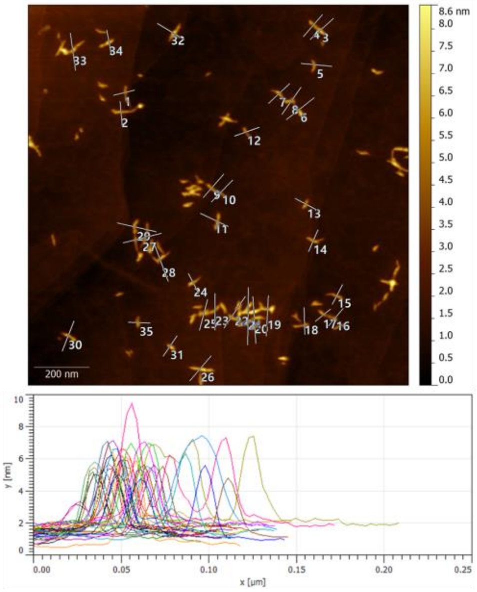

entry	height (nm)
1	3.4
2	4.1
3	5.2
4	3.2
5	4.1
6	3.8
7	4.6
8	4.7
9	4.4
10	4.1
11	4.2
12	3.4
13	3.4
14	3.6
15	3.9
16	4.6
17	3.9
18	4.3
19	3.7
20	7.3
21	5.1
22	4
23	5.2
24	5
25	5.3
26	4.4
27	3.4
28	4.6
29	4.4
30	4.9
31	4.4
32	3.5
33	4.9
34	4
35	3.3
36	5
37	4.8
38	5.9
39	4.8
40	5
41	4.4
avg	**4.4**
std	**0.8**

o-tolyl-P3HT$_{50}$-*b*-PT$_{40}$ (Table 1, entry 5)

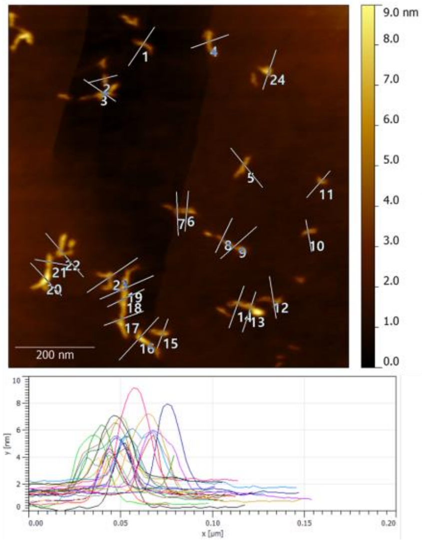

entry	height (nm)
1	5
2	4.2
3	3.7
4	4.5
5	6.8
6	4.7
7	5.2
8	4
9	6.6
10	4.6
11	4
12	4.7
13	2.8
14	2.7
15	3.8
16	3.7
17	2.9
18	2.2
19	3.7
20	3.2
21	3.9
22	4.5
23	5
24	4
25	4.7
avg	**4.2**
std	**1.1**

o-tolyl-P3HT$_{50}$-*b*-PT$_{60}$ (Table 1, entry 6)

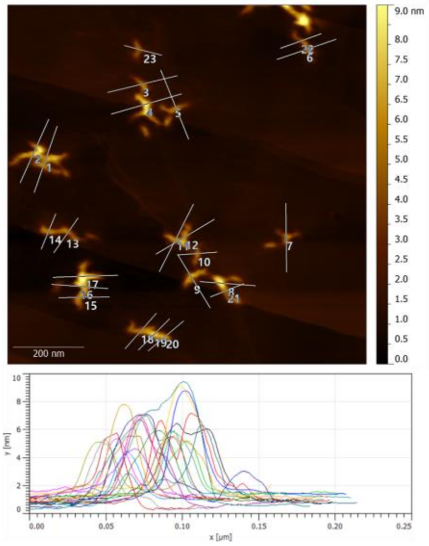

entry	height (nm)
1	3.2
2	3.4
3	4.3
4	5.8
5	6.7
6	4.4
7	8.9
8	6.6
9	4.9
10	5.4
11	4.3
12	6.2
13	5.1
14	4.9
15	6.0
16	7.3
17	4.3
18	4.6
19	4.5
20	7.9
21	3.8
22	5.6
23	6.2
24	5.5
25	5.1
avg	**5.4**
std	**1.4**

o-tolyl-P3HT$_{50}$-*b*-PT$_{60}$ (Table 1, entry 7)

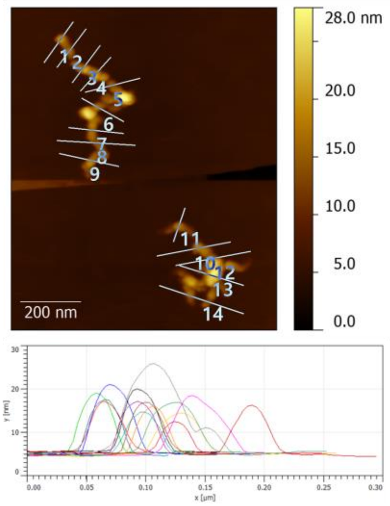

entry	height (nm)
1	7.4
2	10.9
3	20.6
4	11.2
5	12.5
6	14
7	12
8	9.5
9	10.8
10	11.9
11	9.7
12	15.6
13	13.8
14	11.5
15	14.5
avg	**12.4**
std	**3.1**

Figure S5. Estimation of the probability for bidirectional propagation of PT block during conventional KCTP of P3HT-*b*-PT

(1) Probability for the unidirectional propagation of polythiophene homopolymer[11b]

$P(N) = N^{\delta-1}$ (where N = degree of polymerization (DP) and δ = stickiness)

(2) For block copolymerization of P3HT-*b*-PT, probability for the unidirectional propagation of PT block from living chain-end of P3HT[10c]

$P_{\text{P3HT-}b\text{-PT}} = P(N + M)/P(N) = ((N + M)/N)^{\delta-1}$ (where N = DP of P3HT and M = DP of PT)

M	$P_{\text{P3HT-}b\text{-PT}}$ ($\delta = 0.6$)[11b]	$P_{\text{P3HT-}b\text{-PT}}$ ($\delta = 0.68$)[10c]
0	1.00	1.00
40	0.79	0.83
60	0.73	0.78
80	0.68	0.74

(Set N = 50 for P3HT and δ = 0.6 (or 0.68) for P3HT and PT. Note that measurement of δ for PT was impossible due to the high insolubility of PT)

Figure S6. UV-vis spectra of P3HT, P3HT-*b*-PT, and *o*-tolyl-P3HT-*b*-PT films cast from $CHCl_3$

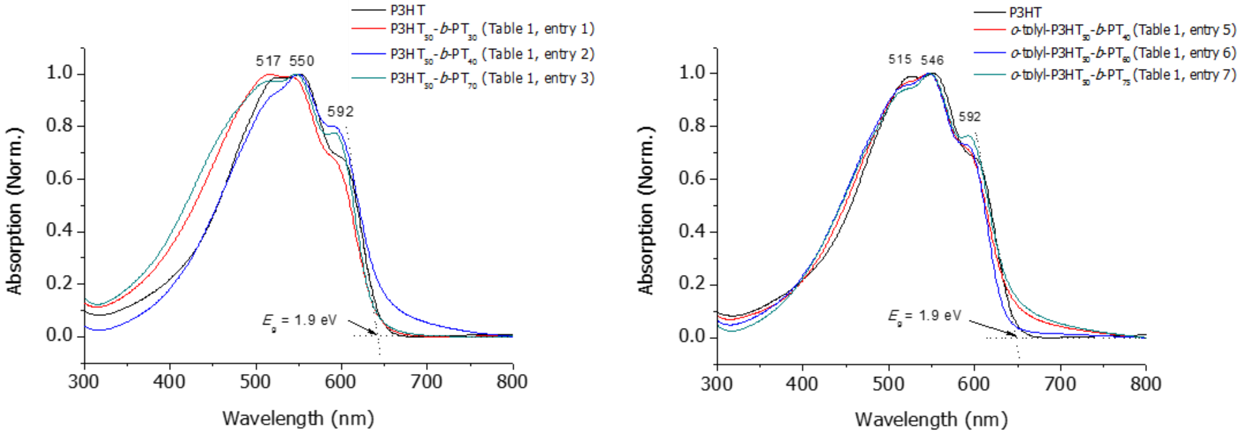
(a) P3HT and P3HT-*b*-PT

(b) P3HT and *o*-tolyl-P3HT-*b*-PT

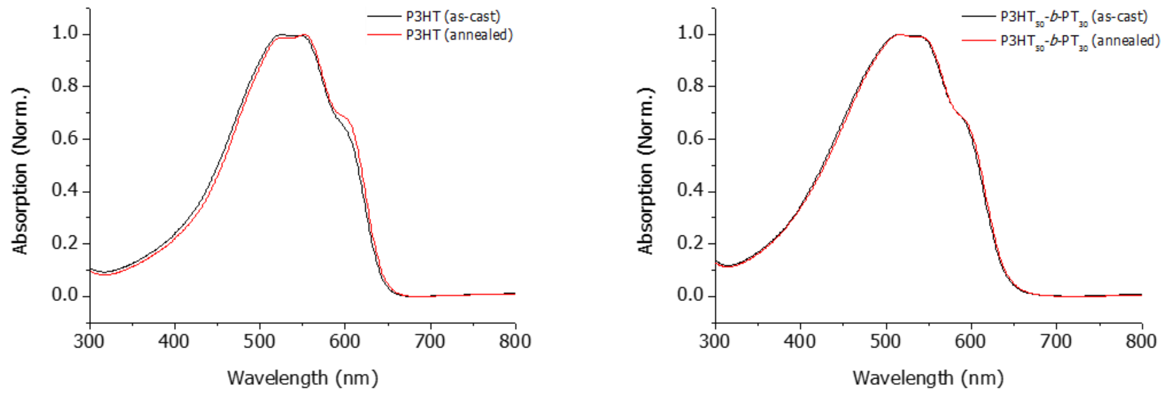
(c) P3HT

(d) $P3HT_{50}$-*b*-PT_{30} (Table 1, entry 1)

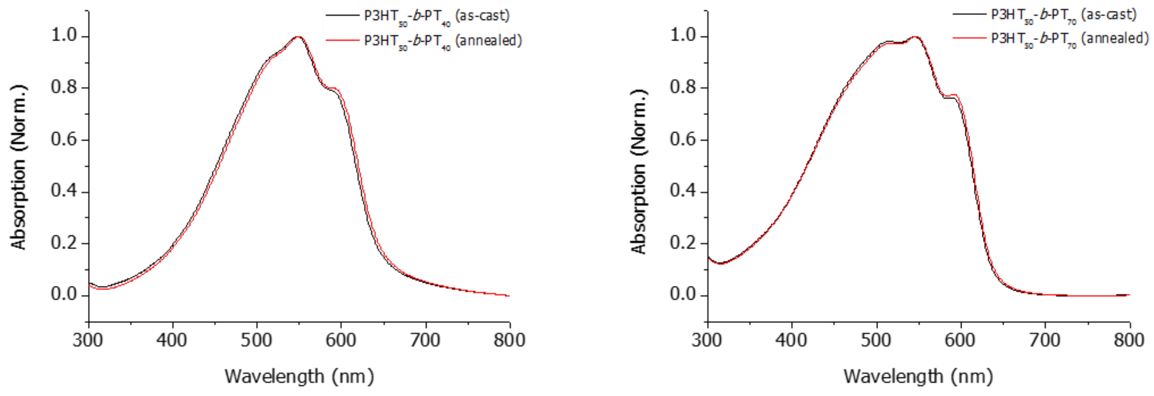
(e) $P3HT_{50}$-*b*-PT_{40} (Table 1, entry 2)

(f) $P3HT_{50}$-*b*-PT_{70} (Table 1, entry 3)

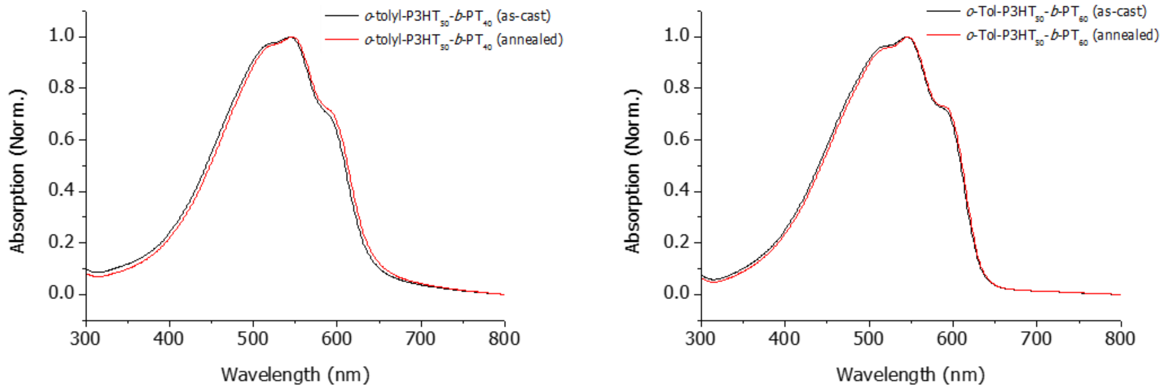

(g) *o*-tolyl-P3HT$_{50}$-*b*-PT$_{40}$ (Table 1, entry 5)

(h) *o*-tolyl-P3HT$_{50}$-*b*-PT$_{60}$ (Table 1, entry 6)

(i) *o*-tolyl-P3HT$_{50}$-*b*-PT$_{75}$ (Table 1, entry 7)

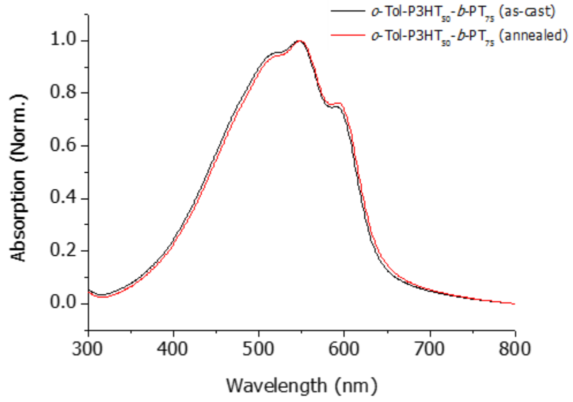

As-cast films were annealed at 150 °C for 10 min

Figure S7. DSC profiles of P3HT, P3HT-*b*-PT, and *o*-tolyl-P3HT-*b*-PT

	T_m	T_c	ΔH_m (J/g)	ΔH_c (J/g)	Corrected ΔH_m (J/g)	Corrected ΔH_c (J/g)
P3HT	231 °C	203 °C	19	20	19	20
P3HT$_{50}$-*b*-PT$_{30}$ (Table 1, entry 1)	206 °C	176 °C	8	9	10	11
P3HT$_{50}$-*b*-PT$_{40}$ (Table 1, entry 2)	212 °C	170 °C	6	7	8	9
P3HT$_{50}$-*b*-PT$_{70}$ (Table 1, entry 3)	194 °C	169 °C	2	2	3	4
o-tolyl-P3HT$_{50}$-*b*-PT$_{40}$ (Table 1, entry 5)	211 °C	169 °C	7	7	10	10
o-tolyl-P3HT$_{50}$-*b*-PT$_{60}$ (Table 1, entry 6)	215 °C	180 °C	9	9	14	14
o-tolyl-P3HT$_{50}$-*b*-PT$_{75}$ (Table 1, entry 7)	216 °C	189 °C	8	8	14	14

$$Correction\ of\ enthalpy = \frac{original\ enthalpy}{gram\ of\ 1st\ block\ P3HT\ from\ 1\ gram\ of\ P3HT-b-PT}$$

P3HT

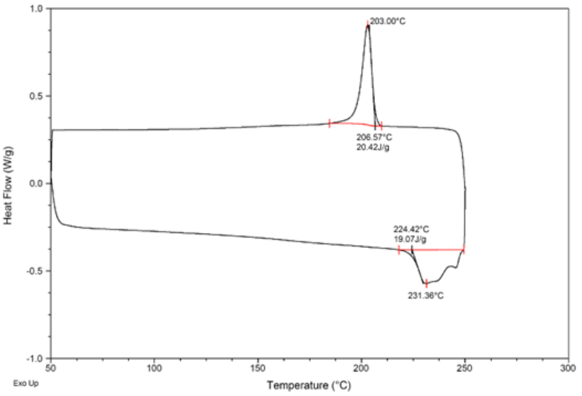

P3HT$_{50}$-*b*-PT$_{30}$ (Table 1, entry 1)

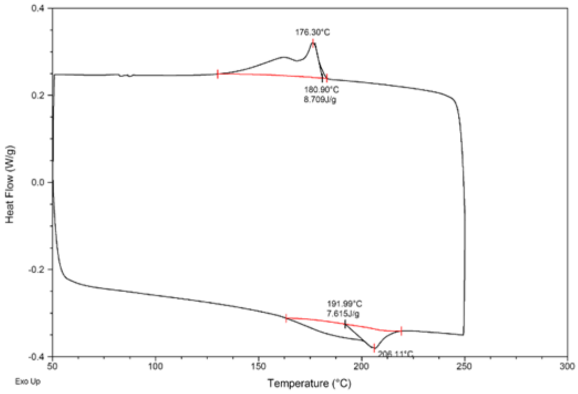

P3HT$_{50}$-*b*-PT$_{40}$ (Table 1, entry 2)

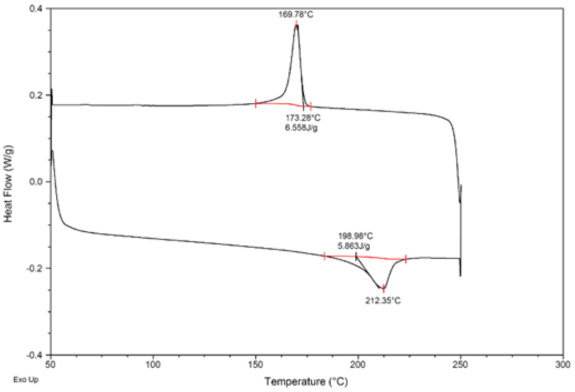

P3HT$_{50}$-*b*-PT$_{70}$ (Table 1, entry 3)

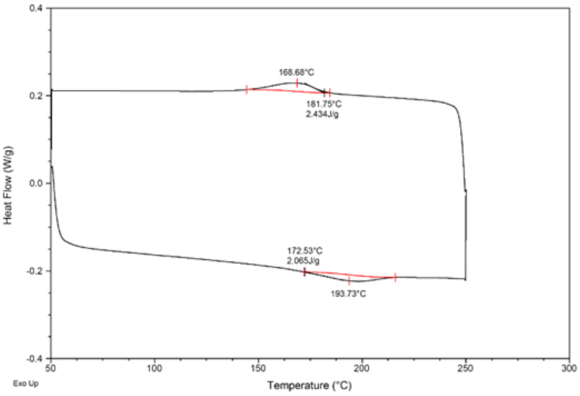

o-tolyl-I-P3HT$_{50}$-*b*-PT$_{40}$ (Table 1, entry 5)

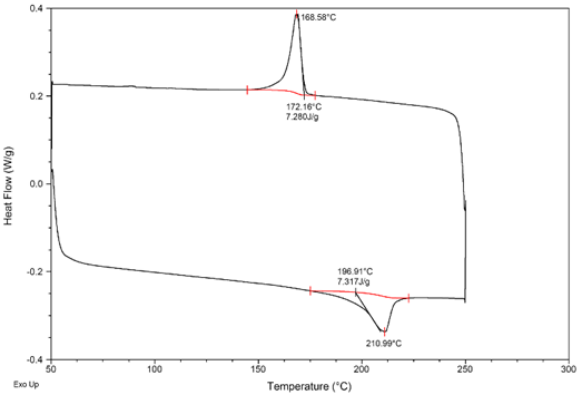

o-tolyl-I-P3HT$_{50}$-*b*-PT$_{60}$ (Table 1, entry 6)

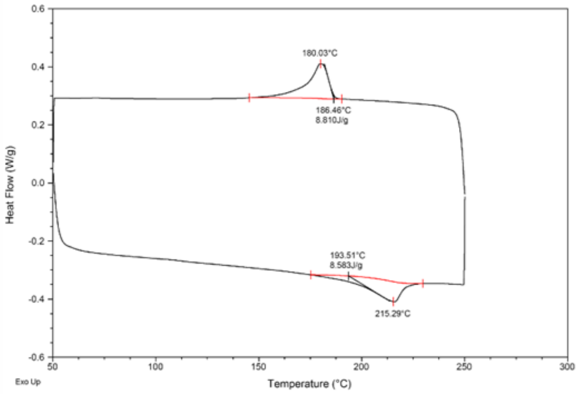

o-tolyl-I-P3HT$_{50}$-*b*-PT$_{75}$ (Table 1, entry 7)

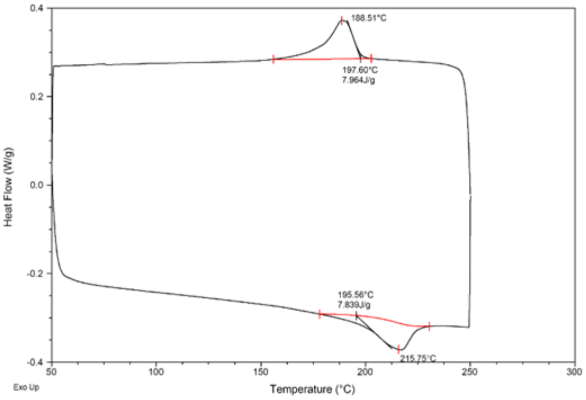

1st cycle for crystallization and 2nd cycle for melting

Figure S8. Powder XRD patterns of P3HT, PT, P3HT-*b*-PT, and *o*-tolyl-P3HT-*b*-PT

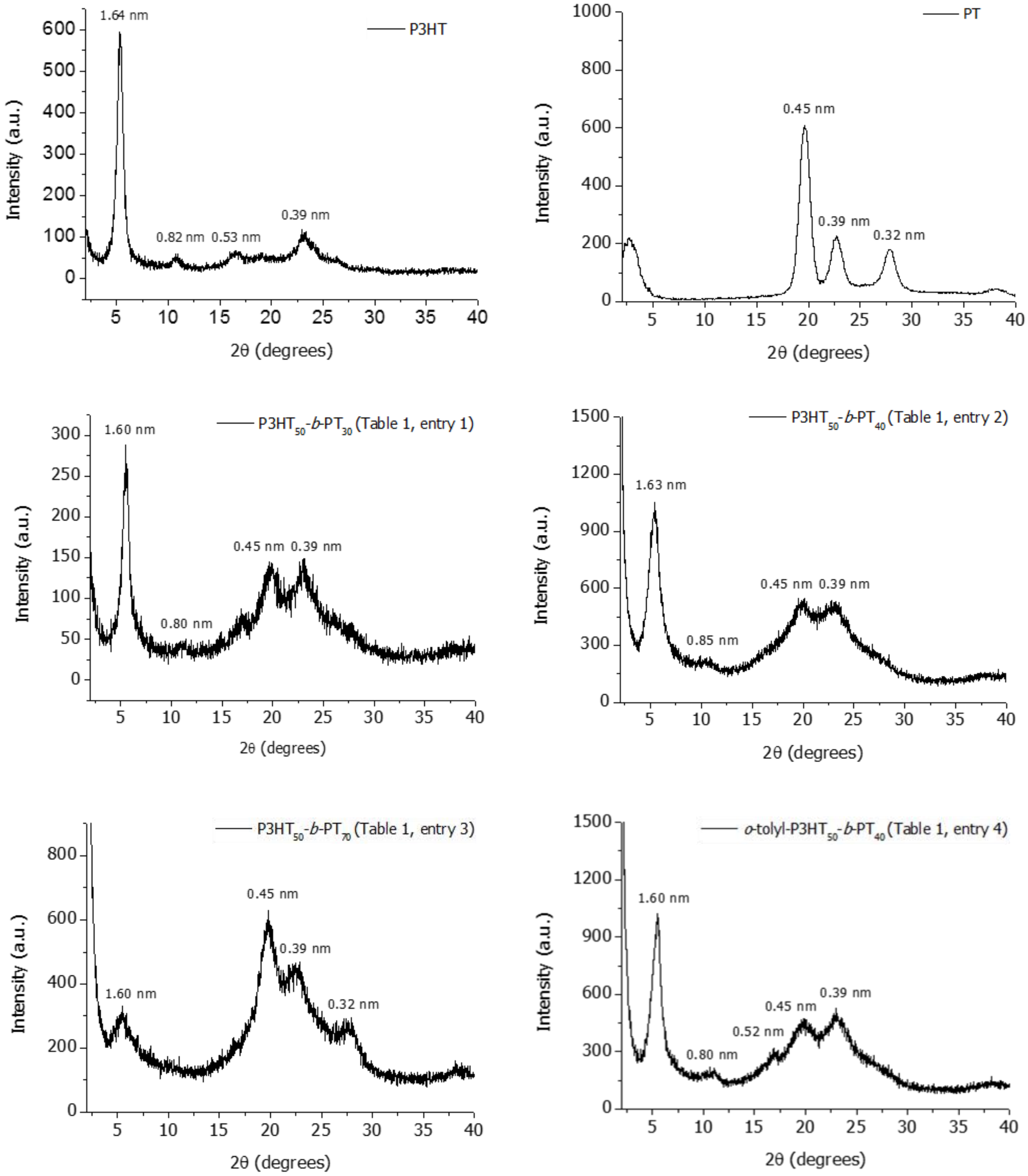

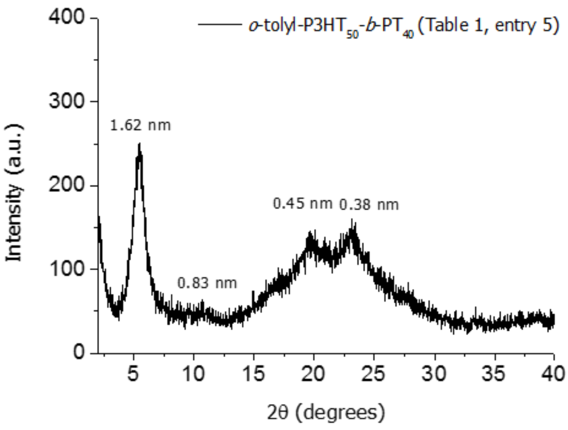

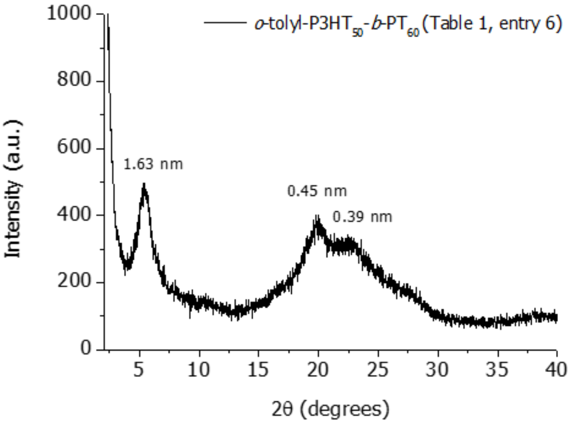

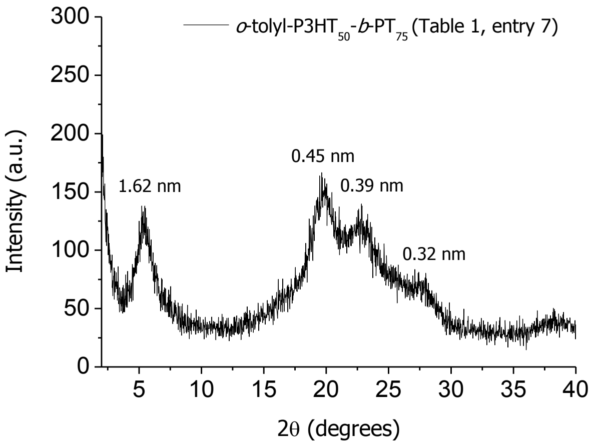

Figure S9. HOMO and LUMO energy levels of P3HT, P3HT-*b*-PT, and *o*-tolyl-P3HT-*b*-PT

	optical E_g (eV)	HOMO (eV)[a]	LUMO (eV)[b]
P3HT	1.9	-5.1	-3.2
P3HT$_{50}$-*b*-PT$_{30}$ (Table 1, entry 1)	1.9	-5.2	-3.3
P3HT$_{50}$-*b*-PT$_{40}$ (Table 1, entry 2)	1.9	-5.2	-3.3
P3HT$_{50}$-*b*-PT$_{70}$ (Table 1, entry 3)	1.9	-5.3	-3.4
o-tolyl-P3HT$_{50}$-*b*-PT$_{40}$ (Table 1, entry 5)	1.9	-5.2	-3.3
o-tolyl-P3HT$_{50}$-*b*-PT$_{60}$ (Table 1, entry 6)	1.9	-5.2	-3.3
o-tolyl-P3HT$_{50}$-*b*-PT$_{75}$ (Table 1, entry 7)	1.9	-5.2	-3.3

[a] HOMO level = -4.8 - ($E_{ox,onset}$ - $Fc^{1/2}$), [b] LUMO level = HOMO level + optical E_g, where $Fc^{1/2}$ = 0.19

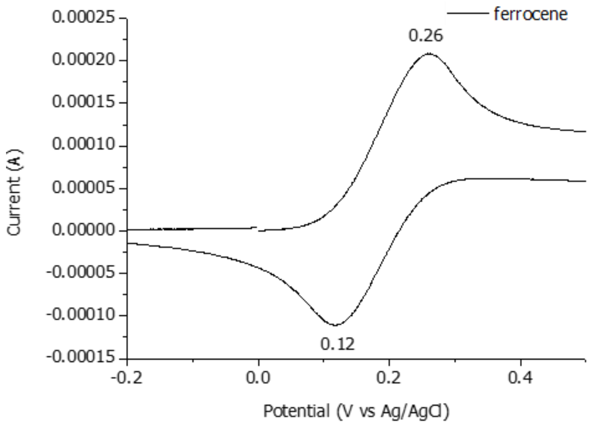
ferrocene
0.26
0.12
Current (A)
0.00025
0.00020
0.00015
0.00010
0.00005
0.00000
-0.00005
-0.00010
-0.00015
-0.2
0.0
0.2
0.4
Potential (V vs Ag/AgCl)

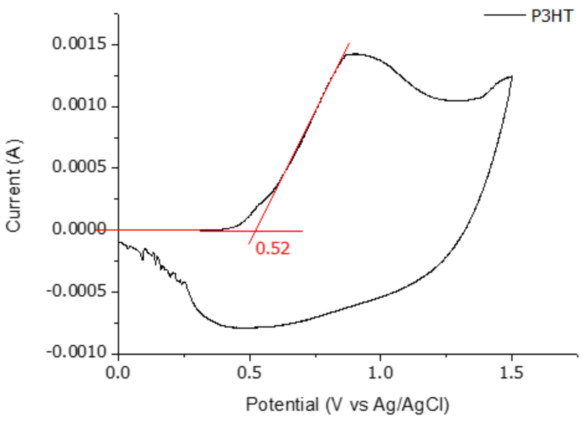
P3HT
0.52
Current (A)
0.0015
0.0010
0.0005
0.0000
-0.0005
-0.0010
0.0
0.5
1.0
1.5
Potential (V vs Ag/AgCl)

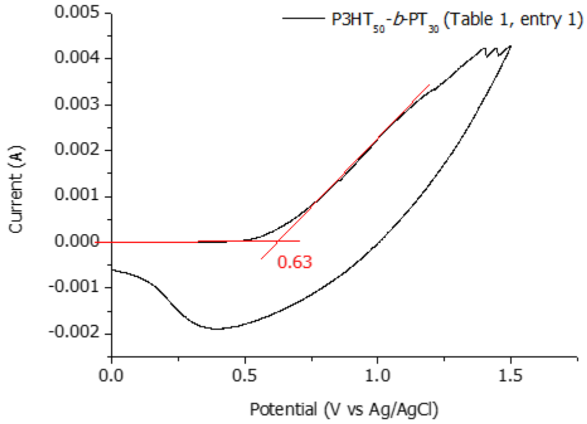
P3HT$_{50}$-*b*-PT$_{30}$ (Table 1, entry 1)
0.63
Current (A)
0.005
0.004
0.003
0.002
0.001
0.000
-0.001
-0.002
0.0
0.5
1.0
1.5
Potential (V vs Ag/AgCl)

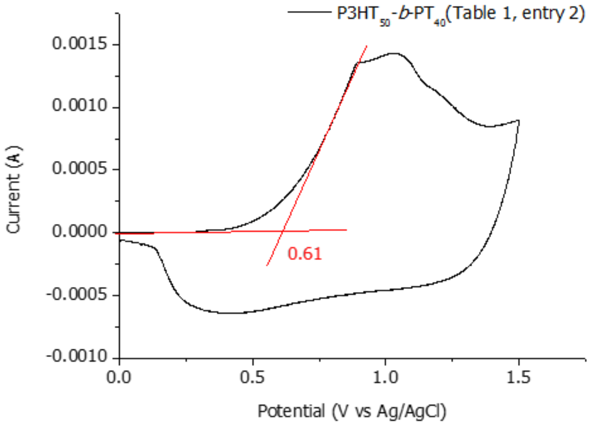
P3HT$_{50}$-*b*-PT$_{40}$(Table 1, entry 2)
0.61
Current (A)
0.0015
0.0010
0.0005
0.0000
-0.0005
-0.0010
0.0
0.5
1.0
1.5
Potential (V vs Ag/AgCl)

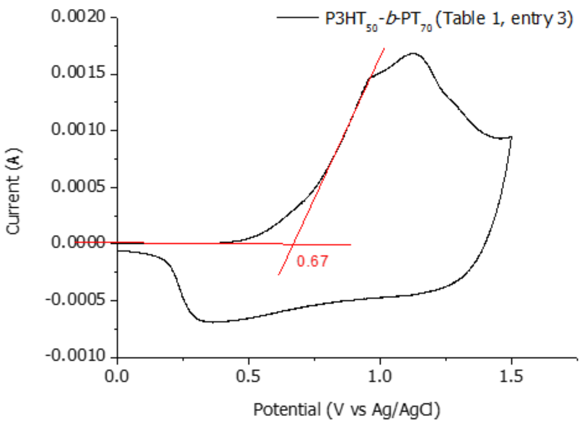
P3HT$_{50}$-*b*-PT$_{70}$(Table 1, entry 3)
0.67
Current (A)
0.0020
0.0015
0.0010
0.0005
0.0000
-0.0005
-0.0010
0.0
0.5
1.0
1.5
Potential (V vs Ag/AgCl)

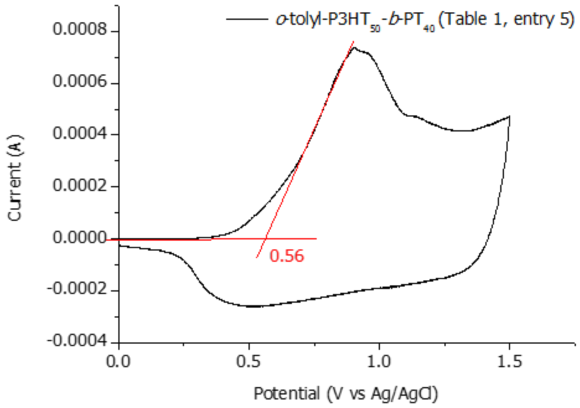
o-tolyl-P3HT$_{50}$-*b*-PT$_{40}$(Table 1, entry 5)
0.56
Current (A)
0.0008
0.0006
0.0004
0.0002
0.0000
-0.0002
-0.0004
0.0
0.5
1.0
1.5
Potential (V vs Ag/AgCl)

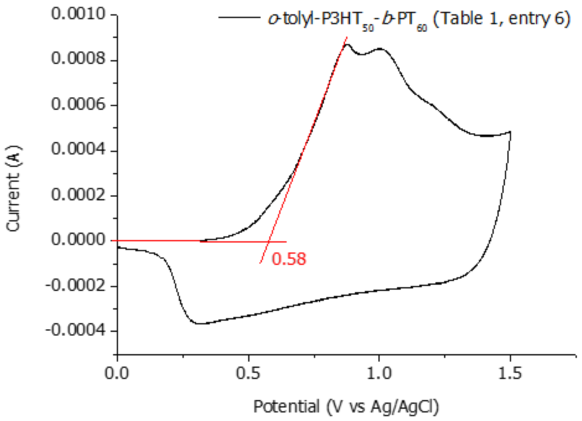

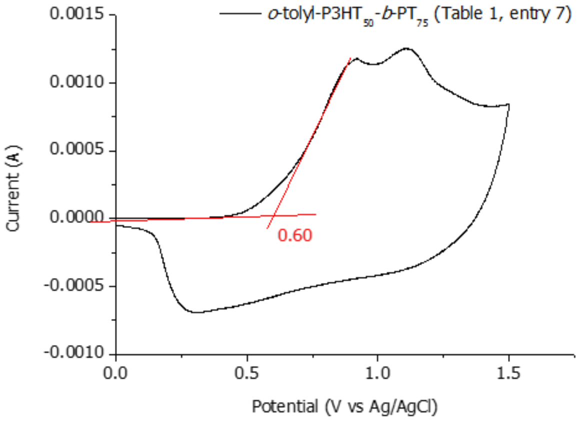

References

(S1) A. C. J. Heinrich, B. Thiedemann, P. J. Gates and A. Staubitz, *Org. Lett.*, 2013, **15**, 4666.

(S2) U. Beckmann, G. Hägele and W. Frank, *Eur. J. Inorg. Chem.*, 2010, 1670.

(S3) N. H. Park, G. Teverovskiy and S. L. Buchwald, *Org. Lett.*, 2014, **16**, 220.